Fractal growth in hydrodynamic dispersion through random porous media

Nicos S. Martys
National Institute of Standards and Technology, Building Materials Division, Gaithersburg, Maryland 20899
(Received 23 November 1993)

Results from the numerical simulation of hydrodynamic dispersion in model random porous media are presented. The morphology of a spreading dye (or tracer), as a function of Peclet number, is studied. In the limit of infinite Peclet number, the dye pattern formed is fractal with fractal dimension close to that observed in diffusion-limited aggregation (DLA) in both two and three dimensions. Also, as in DLA, multifractal behavior is exhibited. At moderately high Peclet numbers the pattern formed by the dispersing dye in a two-dimensional porous medium is fractal over the width of the front as observed in experiment. In the low Peclet number regime contours of equal concentration are self-affine with an anomalously large roughness exponent. By comparison, we show that the pattern formed by a dilute ion concentration driven by an electric field, rather than a flow field, is also self-affine but with the usual roughness exponent of 0.5.

PACS number(s): 47.55.Mh

I. INTRODUCTION

The flow of fluids through random porous media plays an important role in a wide variety of environmental and technological processes. Examples include the spread of hazardous waste in soils, the displacement of oil in petroleum engineering, and separation processes such as chromatography and catalysis. Studies of both miscible and immiscibe fluid invasion in porous media have revealed a wealth of interesting growth morphologies such as compact, invasion percolation and diffusion-limited aggregation (DLA) growth [1–21]. Such diverse behavior is the result of a variety of growth mechanisms which depend on the fluid properties, the structure of the porous medium, and the external driving force which displaces the fluids.

Suppose a porous medium is saturated with a Newtonian fluid. A pressure gradient is applied across the medium maintaining steady flow. The fluid flow is assumed to be divergenceless and in the limit of low Reynolds number. If we now introduce a miscible dye at the side from which the fluid is entering, the dispersion or spread of the dye is locally described by the advection-diffusion equation [20, 19]

$$\frac{\partial c}{\partial t} + \mathbf{v} \cdot \nabla c = D_m \nabla^2 c. \tag{1}$$

Here c is the concentation of the dye, $\mathbf{v}$ is the local fluid velocity, and D_m is the molecular diffusion constant. A dimensionless number which is useful to characterize the competition between diffusion and advection in the spread of a dye is the Peclet number [20] Pe= $\langle v \rangle l / D_m$ where $\langle v \rangle$ is the average fluid speed and l is a length scale which depends on the pore geometry. When Pe is small, the diffusion process dominates the spread of the dye; at large Pe, advection dominates.

At length scales much larger than the typical pore size, hydrodynamic dispersion is generally described by the macroscopic advection-diffusion equation [20]

$$\frac{\partial C}{\partial t} + \mathbf{V} \cdot \nabla C = D_L \frac{\partial^2 C}{\partial x^2} + D_T \frac{\partial^2 C}{\partial y^2}, \tag{2}$$

where C is the macroscopic mean concentration, D_L and D_T are the longitudinal and transverse dispersion coefficients, respectively, $\mathbf{V}$ is the macroscopic mean velocity, and x is in the direction of the mean flow. The macroscopic advection-diffusion equation is valid when the squared width of the dispersion front scales linearly with time. When the squared width scales nonlinearly, dispersion is called anomalous [13, 15].

Previous theoretical work [11, 13–15] concerning scaling in hydrodynamic dispersion through a disordered porous medium has largely focused on the understanding of anomalous dispersion and the prediction of D_L and D_T as a function of Pe and pore geometry. Here, considerable progress [11] has been made by applying percolation [11] concepts to dispersion in random network models of porous media or by direct simulation of dispersion [14], at the pore scale, via the numerical solution of Eq. (1).

Recently, experiments by Måløy *et al.* [18] have found a new morphological feature of a fluid undergoing hydrodynamic dispersion in random porous media. They showed that equal concentration contours resulting from the displacement of a clear fluid, by a colored fluid with the same viscosity exhibited fractal scaling. It was argued that because hydrodynamic dispersion does not have an intrinsic length scale between the size of the pore and the width of the front, which diverges with time, it is reasonable to expect fractal scaling [18] over this range. However, since the experimental results described by Måløy *et al.* were over a limited range of Pe, it is not clear what role Pe should have in controlling the morphology of the dispersing front.

In general, the numerical study of pattern formation and fractal scaling in fluid invasion of porous media [12, 4–6] has focused on immiscible fluids. These studies are typically in the quasistatic regime where capillary forces dominate viscous ones. In the most widely

studied model of fluid invasion, invasion percolation [12], the porous medium is mapped onto a network of nodes and bonds where nodes correspond to pores and bonds correspond to throats which connect the "larger" pores. The invading fluid is allowed to pass through the throats and pores depending on the given pressure drop and the wetting properties of the fluid. In these simulations self-similar fractal scaling is observed as the invading fluid forms a percolating pattern across the porous medium. Results from more detailed simulations of fluid invasion [10, 4], where the wetting properties of the fluids have been explicity included, exhibit self-similar and self-affine scaling depending on whether the invading fluid is non-wetting or wetting, respectively [4, 5].

In this paper, results are presented of a theoretical study of pattern formation associated with the hydrodynamic dispersion of a dye (or tracer) as a function of Pe in two- and three-dimensional random porous media. From the numerical simulation of hydrodynamic dispersion at the pore scale, it is found that tracer dispersion through a random porous medium exhibits a fractal or self-affine growth morphology depending on whether advection or diffusion controls the spread of the dye. In the limit of pure advection, or infinite Pe, the fractal dimension of the pattern formed by an invading dye is close to that of DLA. At intermediate Pe, as suggested by experiments by Måløy *et al.* [18], the morphology of the region defined by a threshold of dye concentration exhibited fractal scaling but with fractal dimension greater than DLA. In the low Pe regime the pattern formed by the invading dye was found to be self-affine with an anomalously large roughness exponent. Since it is quite common to draw an analogy between fluid flow [22] and flow of electrical current in porous media, results from dispersion due to an electrically driven dilute concentration of ions are given for comparison. Again, the morphology of equal concentration contours of ions was found to be self-affine, but with a roughness exponent different from that determined in the fluid driven case (for $\mathrm{Pe} \neq 0$). Results from these simulations are compared to scaling behavior found in studies of immiscible displacement of fluids.

Section II summarizes the numerical techniques and describes the modeled porous media studied. Section III presents results of simulations. Finally, Sec. IV further discusses the results and presents conclusions.

II. NUMERICAL CALCULATIONS

A. Models of porous media

Most of this paper will focus on dispersion through two-dimensional porous media constructed by randomly placing digitalized disks on a lattice such that they do not overlap. The disks have diameter 11, in units of lattice spacing, and the number of packed disks is such that the porosity $\phi = 0.8$. Typical system size was 300×300. For a qualitative comparison of hydrodynamic dispersion in different porous media, cases where the porosity is very high (dilute concentration of disks) and where the porosity is near a percolation threshold are also considered. In the former case the porous medium is constructed with nonoverlapping disks having diameter 11 but with $\phi = 0.95$ and in the latter, the porous medium is constructed by randomly overlapping disks of diameter 23 such that $\phi = 0.4$. In addition, dispersion in the infinite Pe limit for the case of flow through a three-dimensional porous medium was studied for a porous medium constructed by randomly parking nonoverlapping digitalized spheres. The system size was 100^3, and equal numbers of spheres having diameters 15, 11, 7, and 3 were used, resulting in $\phi = 0.528$.

B. Summary of numerical methods

1. *Fluid flow*

In the limit of slow incompressible flow, steady state fluid flow is described by the linear Stokes [20] equations

$$\eta \nabla^2 \mathbf{v}(\mathbf{r}) = \nabla p(\mathbf{r}), \tag{3a}$$

$$\nabla \cdot \mathbf{v}(\mathbf{r}) = 0, \tag{3b}$$

where $\mathbf{v}$ and p are, respectively, the local velocity and pressure fields, η is the fluid viscosity, and $\mathbf{r}$ is the location. The fluid velocity must vanish at pore/solid interfaces and a pressure difference is applied at the inlet and outlet faces. To numerically solve the Stokes equations, we use a finite-difference scheme in conjunction with the artificial compressibility relaxation algorithm [23, 24]. The pore space is discretized into a marker-and-cell (MAC) mesh [24], where pressures are defined at the nodes and fluid velocity components are defined along the center of bonds connecting nodes. Each voxel, a unit square [or cube in three dimensions (3D)], representing either pore or solid, is centered on a node. Near the pore/solid interface, noncentered difference equations are used to improve the accuracy of the solution and to force the fluid velocities to zero at the pore/solid interface. As a result, velocity profiles across voxels are accurate to at least second order [25].

2. *Advection-diffusion*

For finite Pe, the advection-diffusion equation was solved numerically using finite-difference methods [26–30,24]. The local concentration was specified on the nodes of the same MAC mesh used in the fluid flow simulation. An advantage of using the MAC mesh is that it naturally forces conservation of matter throughout the porous medium. To improve numerical accuracy and prevent oscillations in concentration which may appear due to steep gradients in concentration, we adopted the Barton [26, 27] scheme in solving the advection-diffusion equation. Periodic boundary conditions were imposed along the sides parallel to the main flow direction. At the outlet the boundary condition $\partial c/\partial x = 0$ was maintained. Initially, the dye concentration is zero throughout the porous medium. A fixed dye concentration is introduced at the inlet and spreads according to Eq. (1) until the pore space is nearly saturated with dye.

A different numerical method was used to examine the infinite Pe limit. Here, a line of point particles (also called tracers), introduced along the inlet, were advanced by using a second order Runge-Kutta [29] method. Off lattice fluid velocities were interpolated to second order accuracy using a Taylor expansion for MAC mesh variables developed by Chan and Street [28]. The accuracy of the interpolation scheme was adequate enough so that, with a small enough time step, a tracer would cross the porous medium and, via periodic boundary conditions, closely approach its initial position.

III. RESULTS

A. Pattern formation as a function of Peclet number

Figure 1 shows dispersion patterns formed by an invading dye for the case where $\phi = 0.8$ and Pe=0, 0.25, 25, and ∞. Here the length scale in Pe is the disk radius. Clearly, at the lowest Pe, diffusion dominates pattern formation. Contours of equal concentration generally form a single-valued function with respect to a line drawn along the

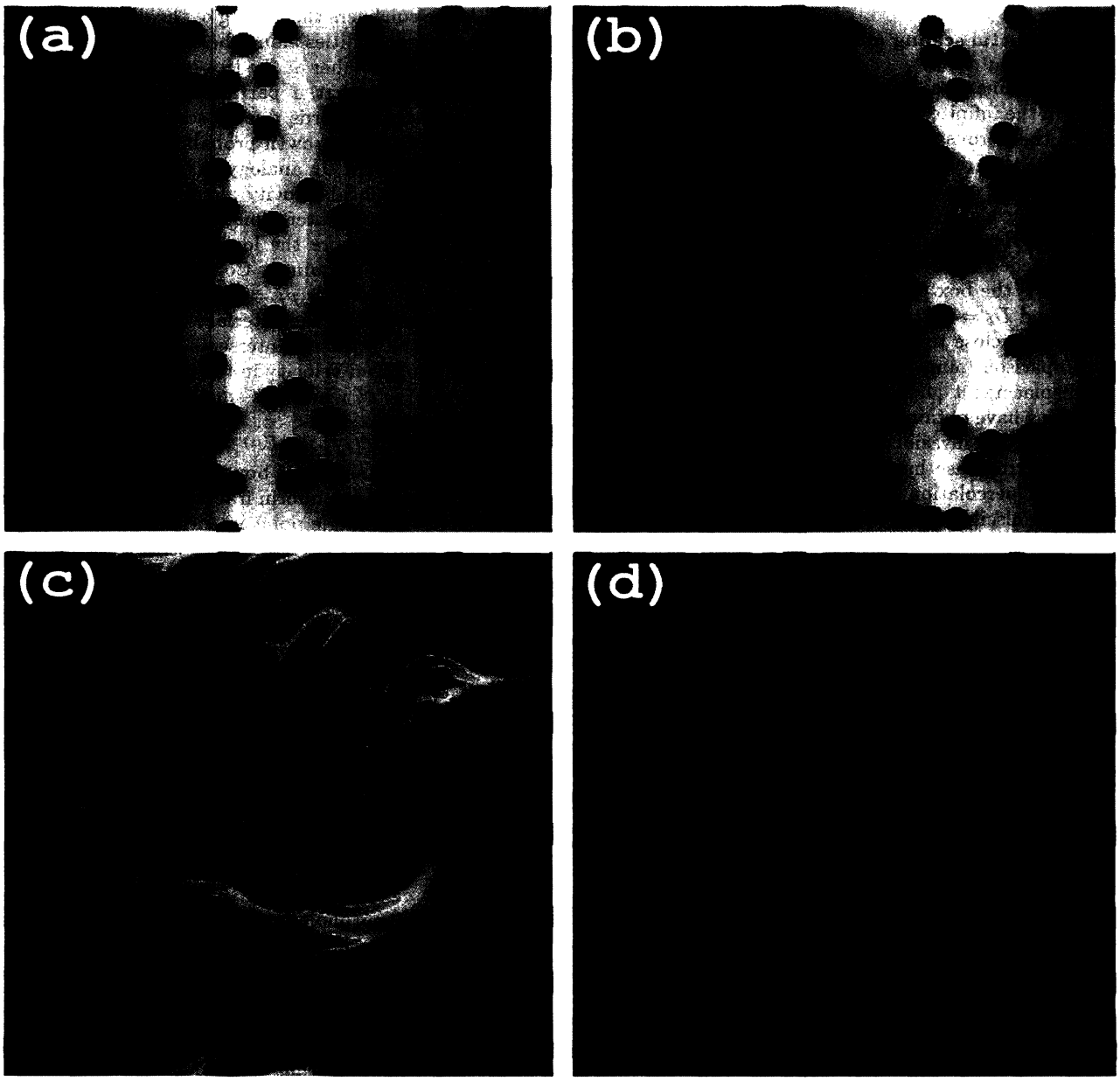

FIG. 1. Panels (a)–(d) show snapshots of different types of pattern formation in hydrodynamic dispersion for Pe=0, 0.25, 25, and ∞, respectively. Dye concentration scales such that blue is $c = 1$ and red $c = 0$. Green areas correspond to $c \approx 0.5$. The porous medium was initially saturated with a red fluid. A blue dye then entered from the left.

inlet. The small local variation in concentration profiles is due to the presence of impenetrable disks and relatively small fluctuations in the velocity fields. As Pe increases, advection begins to dominate and fingers form as the dye advances through channels where the fluid velocity is greatest. Slow flow velocity regions take much longer to invade because the dye enters primarily by diffusion. At infinite Pe, well defined fingers form as the dye follows the winding tortuous path of the fluid. It is striking how the dye tracers can enter the same pore from different starting points, asymptotically approaching each other, and then separate. Experimental studies [31] of hydrodynamic dispersion in etched networks are in qualitative agreement with our simulations.

B. Fractal scaling at Peclet number $= \infty$

To determine the fractal dimension of the pattern formed in the infinite Pe limit, the dye is allowed to move through the porous medium until it first percolates (any part of the dye reaches the outlet). The region that is invaded by the dye is converted into a digital image. A box counting algorithm [2] was used for several infinite Pe images. Here the number of boxes $N(l)$ with sides of length l needed to cover the pattern scales as $N(l) \sim l^{D_b}$, where D_b is the box fractal dimension by definition.

We found $D_b = 1.72 \pm 0.06$ in two dimensions (Fig. 2). This value is close to that obtained in DLA ($D_b \approx 1.7$). For comparison, numerical studies of quasistatic immiscible displacement [4, 5] of one fluid by another in two dimensions have obtained a $D_b \approx 1.88$ and 2 for nonwetting and wetting invasion, respectively. Results similar to the nonwetting case have also been obtained in studies of invasion percolation [6] on a square lattice. In quasistatic immiscible displacement of fluids, the invading front is largely driven by capillary forces as opposed to the viscous flow and diffusion as described in this paper. Therefore, it is not surprising that quasistatic immiscible deplacement of fluids and hydrodynamic dispersion exhibit different fractal scaling.

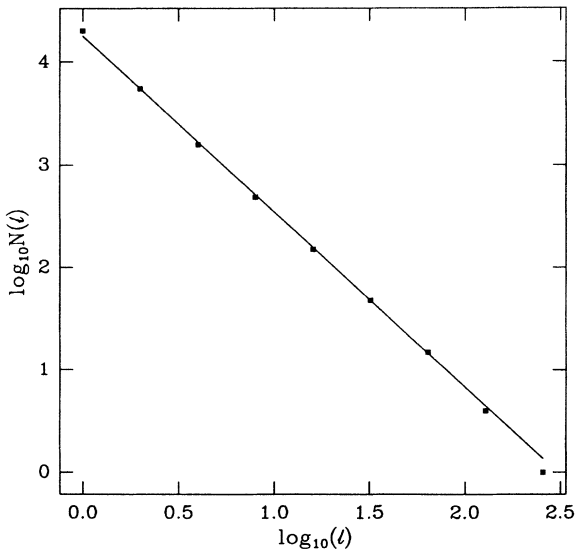

FIG. 2. The log of number of boxes $N(l)$ with side length l needed to cover pattern formed in the Pe=∞ case. The negative of the slope $D_b = 1.72$ is equal to the box dimension and is close to that found in DLA.

We also determined the box dimension of the pattern formed in the three-dimensional porous medium described in Sec. II A. It was found to be consistent with DLA with $D_b = 2.54 \pm 0.05$ (note 2.5 is close to the bulk fractal dimension of both DLA and 3D percolation).

C. Multifractal scaling

Also studied was whether Pe=∞ dispersion, as in DLA, exhibits mutifractal behavior [1, 2]. For instance, in DLA one considers the scaling of the distribution of local growth probabilities along the aggregate front. These probabilities are higher at the tips of the interface (where it is more likely that a particle is captured) and are greatly reduced in fjords due to screening. The spatial distribution of local growth probabilities is known to be multifractal in DLA. In analogy to the DLA local growth probability, the local velocity along the advecting front, which is typically greater along tips of the interface and small in regions where the local configurations of disks restrict flow, was examined. Consider the set of normalized interface velocities $p_j = v_j / \sum_{i=1}^{n} v_i$, where j is the jth grid point along the interface and the sum is over grid points the interface intersects. Define $p_i(\epsilon)$ as the average normalized velocity in the ith region of size ϵ. In general, $p_i(\epsilon) \sim \epsilon^{\alpha}$ where ϵ is small compared to the system size and $-\infty < \alpha < \infty$. The number of boxes with the same α is $N_\alpha(\epsilon) \sim \epsilon^{-f(\alpha)}$, where $f(\alpha)$ is the fractal dimension of the subset of boxes with exponent α. Note that for an ordinary uniform fractal the $f(\alpha)$ spectrum is represented by a single point in the f-α plane whereas a system characterized by a set of α with associated $f(\alpha)$ is described as multifractal. Also, it can be shown that the maxium of $f(\alpha)$ with respect to α is the box dimension of the interface [2]. Following techniques described by Vicsek [2], $f(\alpha)$ was determined for the infinite Pe case. Results are shown in Fig. 3. Clearly the normalized velocities along the dye interface are described by a multifractal set and, as expected, the maximum value of $f(\alpha)$ is approximately the box dimension of the dye pattern as is seen in DLA.

D. Fractal scaling at Peclet number $< \infty$

Måløy *et al.* [18] provided the first experimental evidence that the morphology of a dispersion pattern formed on scales smaller than the width of the dispersion front is fractal. They examined equal concentration contours ($c \approx 0.5$) formed in the displacement through a glass bead pack of a clear fluid by a viscous matched colored fluid. Måløy *et al.* found that the fractal dimension of the concentration front $D_s = 1.42 \pm 0.05$ (where the subscript s indicates the determination of the box dimension of an equal concentration contour). We examine the box dimension of both the invasion front and the pattern formed by the invading dye for the case where Pe= 25.

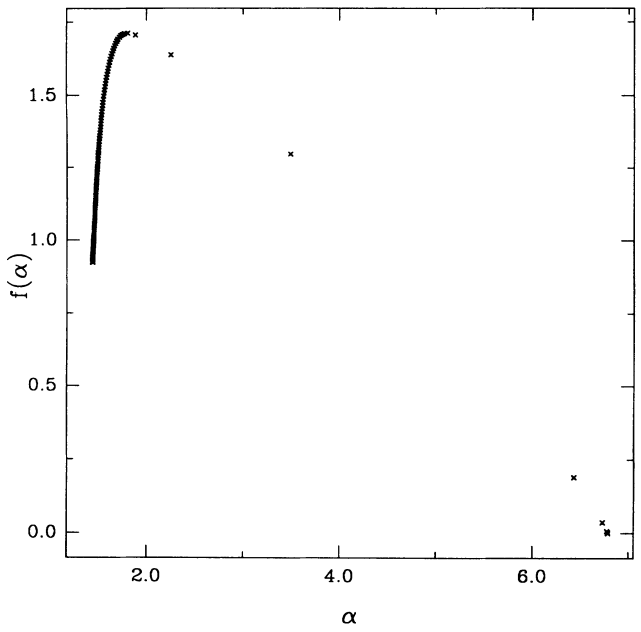

FIG. 3. Plot of the $f(\alpha)$ spectrum associated with normalized velocities along the dye interface. The maximum value of $f(\alpha)$ is close to the box dimension of the dye pattern.

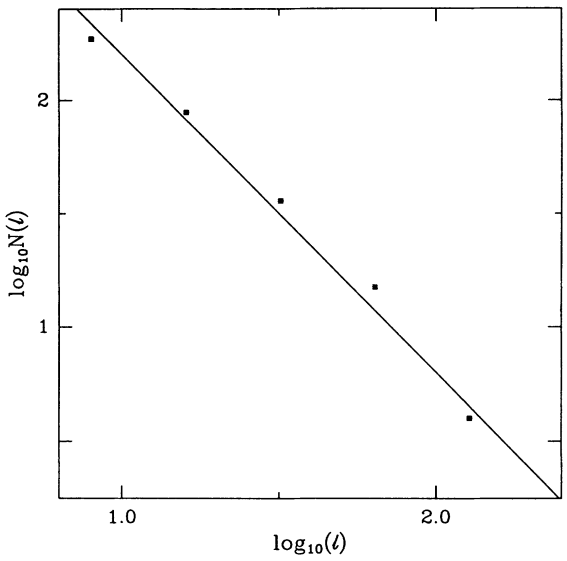

FIG. 4. The log of the number of boxes $N(l)$ needed to cover the front formed by an equal concentration contour where $c \approx 0.5$. The negative of the slope, equal to the box dimension of the front, was $D_s = 1.4 \pm 0.1$. Results here are presented for a single front. Similar results were obtained in other simulations.

To evaluate the fractal dimension of the dispersed dye, the dye was allowed to advance until a region of 0.5 concentration percolated. The image of the invaded region was then digitalized, thresholding it at $c = 0.5$. A box counting algorithm was used to determine the fractal dimension of regions having concentration 0.5 or greater. We found that $D_b = 1.8 \pm 0.05$ when averaged over four realizations. To obtain the fractal dimension of the front, only those points in the image with concentration between 0.49 and 0.5 were retained. As in the analysis of Måløy *et al.*, a box counting algorithm was applied to the image and we obtained $D_s = 1.4 \pm 0.1$ (Fig. 4). This scaling was exhibited over a decade where the lower cutoff was the disk diameter. At smaller length scales D_s appeared to be closer to 1.2. In the future we plan to carry out larger scale simulations to obtain a better estimate of D_s. Although these results are close to that obtained by Måløy *et al.*, we have reservations about whether this simulation actually models their experiment and that the agreement may be fortuitous. For instance, Måløy *et al.* claim their results are valid in two dimensions. However, the actual experiment was performed in three dimensions so that the 0.5 concentration contour from which they determine the fractal dimension is a projection from three to two dimensions. In addition, their porous medium was composed of homogenously packed beads while the system studied here consists of randomly packed disks, and probably has a much larger distribution of pore sizes. Further study is needed to determine the universality of the dispersion front's fractal dimension for different realizations of porous medium and Pe. Nevertheless, it appears that the pattern formed by a dispersing dye is fractal over the width of the front.

E. Self-affine scaling at low Peclet number

In the low Pe regime contours of equal concentration were generally single valued and appear to be self-affine. Here the dye may diffuse around a disk before it advances very far into the neighboring pore space, thus producing a smoother interface with few overhangs. The roughness of the equal concentration contours, determined by the root-mean-squared fluctuation of its height h over horizontial intervals of width l, is

$$w(l) = \sqrt{\langle (h - \langle h \rangle_l)^2 \rangle_l}. \tag{4}$$

For a self-affine fractal $w(l) \sim l^{\beta}$, with roughness exponent $\beta < 1$ by definition [2].

At Pe= 0, or pure diffusion, we obtained $\beta = 0.48 \pm 0.02$. A roughness exponent of 0.5 appears in a large class of models which describe the evolution of an interface subject to uncorrelated noise, such as ballistic deposition and Eden growth [2]. Such growth models can be described by the Karder-Parisi-Zhang (KPZ) [7] equation

$$\frac{\partial h}{\partial t} = \gamma \nabla^2 h + \frac{\lambda}{2}(\nabla h)^2 + \eta(\mathbf{x}, \mathbf{t}), \tag{5}$$

where h is the interface height, γ is the surface tension, and λ is a constant. The first term on the right produces a smoothing effect in the interface, the second term is needed to account for lateral growth, and the third term represents noise, which depends on the physical process modeled. In the case of Pe= 0, if you imagine yourself moving along with a constant average concentration profile you would see local random perturbations in the con-

stant concentration line due to impinging disks. These pertubations would disappear as the dye diffuses about the disk, mimicking a surface tension effect. So it is easy to see a connection between growth models described by the KPZ equation and these simulations.

Surprisingly, when Pe$\approx$ 0.25, w scaled with a roughness exponent of about 0.75 $\pm$ 0.04 for the *same* pore structure (Fig. 5). This anomalously large roughness exponent is close to that obtained in a completely different invasion process, where an immiscible wetting fluid invades a porous medium, and has been the subject of considerable debate [9, 3]. While it remains to be seen whether there is a mapping between the two problems, this study shows that such scaling is not unique to wetting invasion and that further studies of hydrodynamic dispersion may help improve the understanding of such exponents. For instance, it has been demonstrated that solutions of the KPZ equation, where the noise term has power law spatial or temporal correlations [16, 17] can produce values of β different from 0.5. In these dispersion simulations, correlations in the flow fields, a result of the fluid primarily moving through the set of largest pores that form a connected path, may produce this anomalous behavior. However, at large enough scales, such that the flow is presumably uncorrelated, we expect the usual 0.5 scaling of roughness to develop.

F. Dispersion in other model porous media

As a qualitative illustration of the important role pore structure plays in dispersion, two examples of dispersion are shown, to contrast with the previous simulations. Figure 6(a) shows dispersion in the overlapping disk model where $\phi = 0.4$. Near the percolation threshold only one connected pore path makes a significant contribution to flow. Large pockets or regions where there is negligible fluid flow greatly restrict the ingress of the dye in that pore space. Here, the dye mainly enters these pockets by diffusing through a tortuous path. In this regime, anomalous dispersion [32] is expected to take place.

Results from the opposite extreme, of dispersion in highly porous media, are given for the case of $\phi = 0.95$ and Pe=25 in Fig. 6(b). Clearly the flow fields are cor-

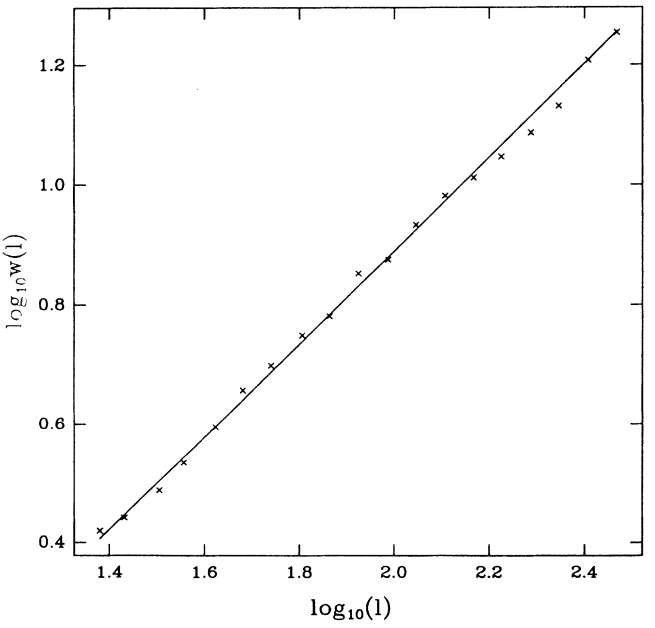

FIG. 5. The scaling of the root-mean-squared fluctuation $w(l)$ of a concentration contour where $c \approx 0.5$. The slope is equal to the roughness exponent $\beta = 0.75 \pm 0.04$.

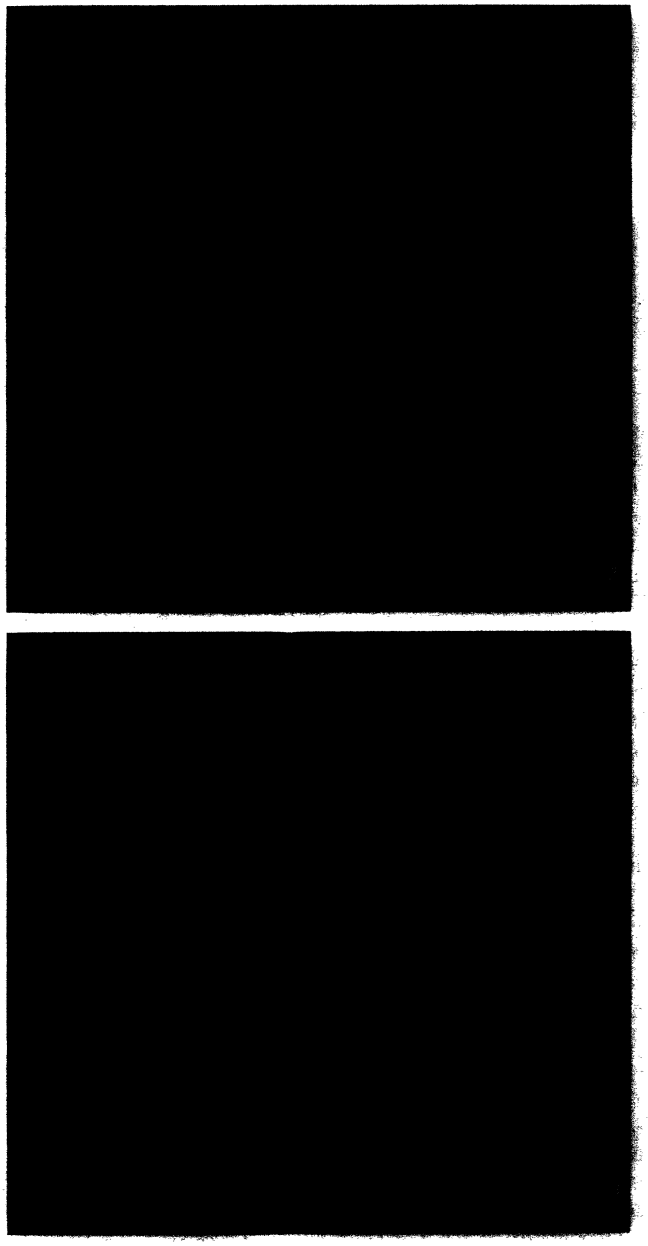

FIG. 6. Examples of dispersion through porous media in the limit where the pore space is near its percolation theshold [panel (a)] and in the opposite limit where the solid fraction is only 5% [panel (b)].

FIG. 7. Electrically driven dispersion of a dilute ion concentration for Pe= 25. Note the dramatic difference in the invasion pattern as compared to Fig. 1(c).

related over very large distances compared to the size of the disk. This leads to the formation of very long and broad fingers. It is surprising, even in this very dilute case, how nonuniform the dispersion front is.

G. Electrically driven concentration

Finally, a comparison is made between the previous dispersion pattern due to fluid flow at Pe= 25 [Fig. 1(c)] and the dispersion of a dilute ion concentration driven by an applied electric field (Fig. 7). Here, the same pore space used in Fig. 1 is filled with a conducting fluid. The disks are assumed to be insulating and uncharged for simplicity [33]. A potential gradient is applied across the system and the Laplace equation is numerically solved to determine the electric potential everywhere. The local electric fields $\mathbf{E}$ are obtained from the negative gradient of the potential. Next, a dilute concentration of ions is introduced at the inlet. The ion velocity is given by $\mathbf{v} = \nu z F \mathbf{E}$ where ν is the ion mobility, z is the ion charge number, and F is Faraday's constant [34]. The dispersion of the ions is then described by Eq. (1) where c represents the ion concentration and $\mathbf{v}$ is the ion velocity as given above.

Clearly, the patterns formed by the two driving forces, for the same Pe, are quite different. It is not unusual to find textbooks [30] that explain fluid flow in terms of electric current and vice versa, and to understand Darcy's law as a type of Ohm's law for fluid flow. However, there are several important differences, at the microscopic scale, between the electric fields and flow fields in these simulations.

Consider first the fluid case. Note that the fluid velocity is zero along the pore/solid boundary. In addition, the solution of Stoke's equation will typically produce a velocity profile, between neighboring disks, that is roughly parabolic. Therefore, there is very little flow in regions only accessible to pores with narrow necks and most of the fluid flow is through the set of largest pores that form a connected path across the porous medium. As a result, a dispersing dye in this porous medium may form long fingers as it moves through the faster channels while slowly entering regions accessible through narrow necks.

In contrast to fluid flow, the calculated electric fields are zero only normal to the solid surface. Also, the solution of the Laplace equation results in an approximately constant electric field along lines perpendicular to the average flow that connect disks. Thus, in the electrically driven case where $\vec{\nabla} \cdot \vec{\mathbf{E}} = 0$, there is significant movement of ions through both the narrow and wide pores such that no portion of the front greatly advances relative to another.

We find that equal concentration fronts driven by the electric field are self-affine. The roughness exponent in this case was about 0.51 ± 0.02 which is smaller than that for the fluid driven case at Pe= 0.25. The ≈ 0.5 exponent is an indication that fluctuations in the equal concentration contours due to the electric fields are *local* (as in the case of Pe= 0) and not correlated over long distances. Further work is needed to see how this result would change at higher Pe and for different pore structures.

IV. SUMMARY

This numerical study has demonstrated the fractal nature of hydrodynamic dispersion in model random porous media. The dye pattern formed in the infinite Pe limit shares many features with DLA, such as fractal and

multi-fractal scaling. As Pe number decreases, the pattern formed in hydrodynamic dispersion appears to show a transition from fractal to self-affine growth (at least at scales up to the width of the front). At low Pe the roughness scales with an anomalously large roughness exponent close to that seen in experiments and simulations of wetting invasion. In contrast, the pattern formed by a dilute ion concentration driven by an electric field was also shown to be self-affine but with a roughness exponent associated with uncorrelated noise.

Further research is needed to determine the effects of finite system size on the results in this work. In addition, more theoretical and experimental work is needed to understand the morphology of a dispersing tracer as a function of pore structure and Pe.

ACKNOWLEDGMENTS

The author would like to thank Dale P. Bentz, Joseph B. Hubbard, Donald Koch, Joel Koplik, and Roland Lenormand for useful conversations, Tere Griffin and Holly Rushmier for assistance in imaging results from simultations, and Ken Snyder for carefully reading over the text.

[1] *Random Fluctuations and Pattern Growth: Experiments Models*, edited by H. E. Stanley and N. Ostrowsky (Kluwer Academic Publishers, Dordrecht, 1988).

[2] T. Vicsek, *Fractal Growth Phenomena* (World Scientific, Singapore, 1989).

[3] *Dynamics of Fractal Surfaces*, edited by F. Family and T. Vicsek (World Scientific, Singapore, 1991).

[4] N. Martys, M. Cieplak, and M. O. Robbins, Phys. Rev. Lett. **66**, 1058 (1991).

[5] N. Martys, M. Cieplak, and M. O. Robbins, Phys. Rev. B **44**, 12 294 (1991).

[6] R. Chandler, J. Koplik, K. Lerman, and J. F. Willemsen, J. Fluid Mech. **119**, 249 (1982).

[7] M. Kardar, G. Parisi, and Y.-C. Zhang, Phys. Rev. Lett. **56**, 889 (1986).

[8] J. P. Stokes, D. A. Weitz, J. P. Gollub, A. Dougherty, M. O. Robbins, P. M. Chaikin, and H. M. Lindsay, Phys. Rev. Lett. **57**, 1718 (1986).

[9] M. A. Rubio, C. Edwards, A. Dougherty, and J. P. Gollub, Phys. Rev. Lett. **63**, 1685 (1989).

[10] M. Cieplak and M. O. Robbins, Phys. Rev. Lett. **60**, 2042 (1988).

[11] Many recent results and important references concerning hyrodynamic dipsersion in porous media are given in articles in *Fractal Dispersion and Diffusion*, edited by John H. Cushman, special issue of Transp. Porous Media **13** (1), 1993. Also see M. Sahimi, Rev. Mod. Phys. **65**, 1393 (1993).

[12] See, e.g., J. Feder, *Fractals* (Plenum, New York, 1988).

[13] M. Sahimi and A. O. Imdakm, J. Phys A **21**, 3833 (1988).

[14] J. Salles, J.-F. Thovert, R. Delannay, L. Prevors, J.-L. Auriault, and P. M. Adler, Phys. Fluids A **5**, 2348 (1993).

[15] S. Redner, J. Koplik, and D. Wilkinson, J. Phys A **20**, 1543 (1987).

[16] Y.-C. Zhang, J. Phys. (Paris) **51**, 2129 (1990).

[17] V. K. Horvath, F. Family, and T. Vicsek, Phys. Rev. Lett. **65**, 1388 (1990).

[18] K. J. Måløy, J. Feder, F. Boger, and T. Jøssang, Phys. Rev. Lett. **61**, 2925 (1988).

[19] Pierre M. Adler, *Porous Media: Geometry and Transports* (Butterworth-Heinemann, Boston, 1992), Chap. 7.

[20] A. E. Scheidegger, *The Physics of Flow Through Porous Media*, 2nd ed. (University of Toronto Press, Toronto, 1974).

[21] A. J. Katz and A. H. Thompson, Phys. Rev. B **34**, 8179 (1986); J. Geophys. Res. **92**, 599 (1987).

[22] E. M. Purcell, *Electricity and Magnetism* (McGraw-Hill, New York, 1965).

[23] N. Martys and E. J. Garboczi, Phys. Rev. B **46**, 6080 (1992).

[24] R. Peyret and T. D. Taylor, *Computational Methods for Fluid Flow* (Springer-Verlag, New York, 1983).

[25] Suppose that, within a given voxel, we were to expand the exact solutions of the Stokes equations $\mathbf{v}(\mathbf{r}) \equiv \mathbf{v}(x, y, z)$ as a Taylor series in x, y, and z. The use of noncentered difference equations guarantees that our solutions properly represent the first three terms of this expansion (i.e., that the errors are of order x^3 or x^2y, etc.).

[26] J. F. Hawley, L. Smarr, and J. R. Wilson, Astrophys. J. Suppl. **55**, 211 (1984).

[27] J. Centralla and J. R. Wilson, Astrophys. J. Suppl. **54**, 229 (1984) .

[28] R. K.-C. Chan and R. L. Street, J. Comput. Phys. **6**, 68 (1970).

[29] W. H. Press, B. P. Flannery, S. A. Teukolsky, and W. T. Vetterling, *Numerical Recipes* (Cambridge University Press, New York, 1989), p. 548.

[30] M. Muscat, *The Flow of Homogeneous Fluids Through Porous Media* (McGraw-Hill, New York, 1937).

[31] R. Lenormand (private communication); E. Charlaix, J.-P. Hulin, C. Leroy, and C. Zarcone, J Phys. D **21**, 1727 (1988).

[32] D. L. Koch and J. Brady, Phys. Fluids A **1**, 47 (1989); S. Redner, J. Koplik, and D. Wilkison, J. Phys. A **20**, 1543 (1987); M. Sahimi and A. O. Imdakm, *ibid.* **21**, 3833 (1988).

[33] The physical assumption of insulating, uncharged disks automatically eliminates the possibility of an electrical double layer. We therefore ignore electrokinetic phenomena associated with hydrodynamic effects which are induced by the interaction of the external field with mobile charges in an "electric double layer" surrounding the disks. For further reference, see Robert J. Hunter, *Zeta Potential in Colloid Science: Principles and Applications* (Academic Press, London, 1981).

[34] R. F. Probstein and R. E. Hicks, Science **260**, 498 (1993).

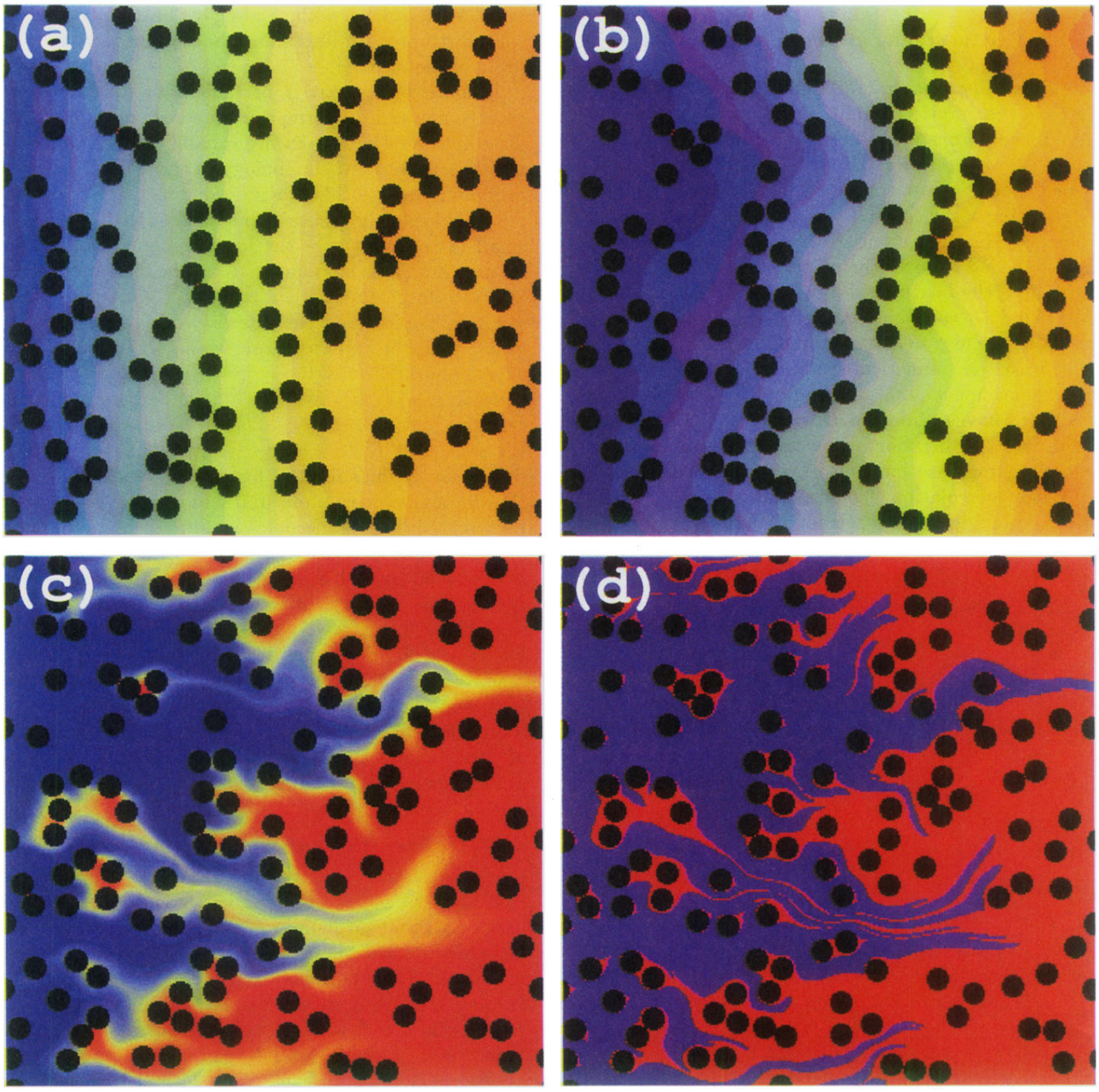

FIG. 1. Panels (a)–(d) show snapshots of different types of pattern formation in hydrodynamic dispersion for Pe=$0, 0.25, 25,$ and ∞, respectively. Dye concentration scales such that blue is $c = 1$ and red $c = 0$. Green areas correspond to $c \approx 0.5$. The porous medium was initially saturated with a red fluid. A blue dye then entered from the left.

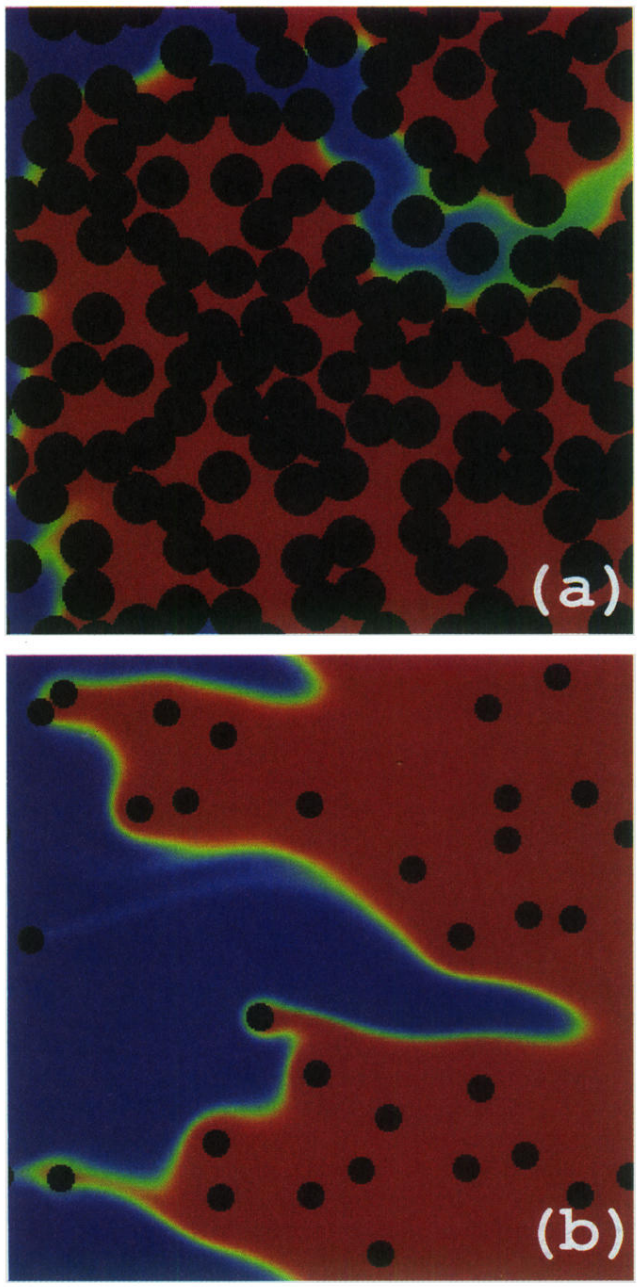

FIG. 6. Examples of dispersion through porous media in the limit where the pore space is near its percolation theshold [panel (a)] and in the opposite limit where the solid fraction is only 5% [panel (b)].

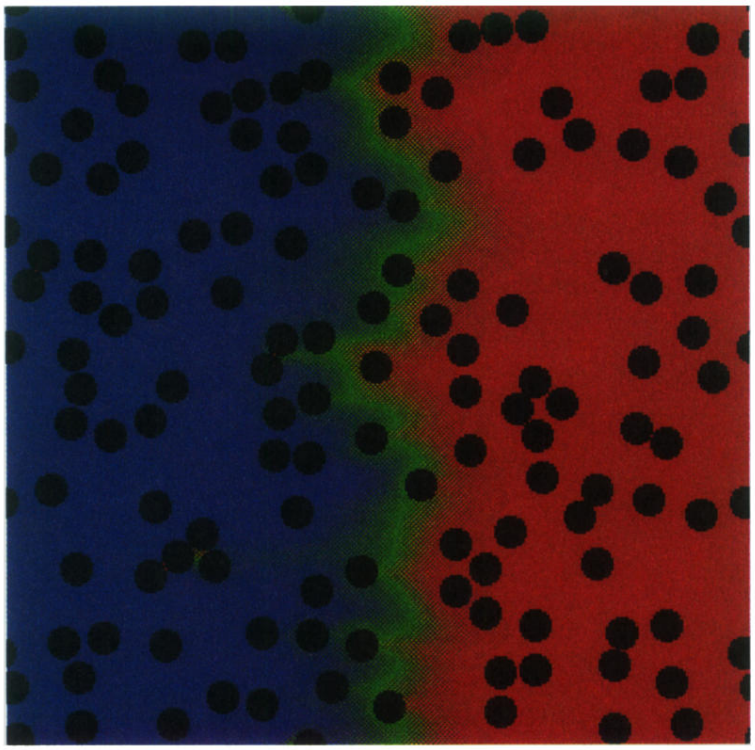

FIG. 7. Electrically driven dispersion of a dilute ion concentration for Pe= 25. Note the dramatic difference in the invasion pattern as compared to Fig. 1(c).